A cautionary tale of Ly C escape fraction estimates from high-redshift galaxies

R. Bassett, E. V. Ryan-Weber, J. Cooke, U. Meštrić, L. J. Prichard, M. Rafelski, I. Iwata, M. Sawicki, S. Gwyn, S. Arnouts

Monthly Notices of the ROYAL ASTRONOMICAL SOCIETY

MNRAS **511,** 5730–5741 (2022) https://doi.org/10.1093/mnras/stac270
Advance Access publication 2022 March 7

A cautionary tale of Ly C escape fraction estimates from high-redshift galaxies

R. Bassett,[1,2]★ E. V. Ryan-Weber,[1,2]★ J. Cooke,[1,2] U. Meštrić,[1,2] L. J. Prichard,[3] M. Rafelski,[3,4] I. Iwata,[5] M. Sawicki,[6]† S. Gwyn[7] and S. Arnouts[8]

[1]*Centre for Astrophysics and Supercomputing, Swinburne University of Technology, PO Box 218, Hawthorn VIC 3122, Australia*
[2]*ARC Centre of Excellence for All Sky Astrophysics in 3 Dimensions (ASTRO 3D), Australia*
[3]*Space Telescope Science Institute, 3700 San Martin Drive, Baltimore, MD 21218, USA*
[4]*Department of Physics & Astronomy, John Hopkins University, Baltimore, MD 21218, USA*
[5]*National Astronomical Observatory of Japan, 2-21-1 Osawa, Mikata, Tokyo 181-8588, Japan*
[6]*Department of Astronomy & Physics and the Institute for Computational Astrophysics, Saint Mary's University, 923 Robie Street, Halifax, Nova Scotia B3H 3C 3, Canada*
[7]*NRC-Hertzberg, 5071 West Saanich Road, Victoria, British Columbia V9E 2E7, Canada*
[8]*Aix Marseille Université, CNRS, LAM - Laboratoire d'Astrophysique de Marseille, 38 rue F. Joliot-Curie, F-13388 Marseille, France*

Accepted 2022 January 27. Received 2022 January 27; in original form 2021 May 31

ABSTRACT

Measuring the escape fraction, $f_{\rm esc}$, of ionizing, Lyman continuum (Ly C) radiation is key to our understanding of the process of cosmic reionization. In this paper, we provide a methodology for recovering the posterior probability distribution of the Ly C escape fraction, $f_{\rm esc}^{\rm PDF}$, considering both the observational uncertainties and ensembles of simulated transmission functions through the intergalactic medium (IGM). We present an example of this method applied to a VUDS galaxy at $z = 3.64$ and find $f_{\rm esc}^{\rm PDF} = 0.51^{+0.33}_{-0.34}$ and compare this to the values computed assuming averaged IGM transmission with and without consideration of detection bias along average sightlines yielding $f_{\rm esc}^{\langle T\rangle} = 1.40^{+0.80}_{-0.42}$ and $f_{\rm esc}^{\rm bias} = 0.82^{+0.33}_{-0.16}$. Our results highlight the limitations of methods assuming average, smooth transmission functions. We also present MOSFIRE data for a sample of seven Ly C candidates selected based on photometric redshifts at $z > 3.4$, but find that all seven have overestimated photometric redshifts by $\Delta z \sim 0.2$ making them unsuitable for Ly C measurements. This results likely due to a bias induced by our selection criteria.

Key words: intergalactic medium – galaxies: ISM – dark ages, reionization, first stars.

1 INTRODUCTION

The epoch of reionization (EoR), the period during which the hydrogen permeating the intergalactic medium (IGM) was photoionized by young galaxies, is currently an extremely active area of research covering a wide range of topics and methods (e.g. Ghara et al. 2021; Hutter et al. 2021; Pagano & Fronenberg 2021). Although our understanding of the timeline of reionization is continually being refined (e.g. Bolton & Haehnelt 2007; Robertson et al. 2015; Planck Collaboration XLVII 2016), there remain a number of key, outstanding questions, such as what are the primary drivers of the reionization process? Inevitably, the ionizing, Lyman continuum (Ly C) photons responsible originate in galaxies: either from stellar sources (e.g. massive O and B stars and X-ray binaries in star-forming galaxies; Eldridge et al. 2017; Shivaei et al. 2018) or from active galactic nuclei (AGNs; e.g. Grazian et al. 2018). Currently star-forming galaxies are favoured while AGNs are expected to play a larger role in sustaining the ultraviolet (UV) background radiation that maintains an ionized IGM at lower redshifts (Kakiichi et al. 2018).

The difficulty in definitively answering the question of which sources are primarily responsible for reionization can be attributed to the faintness of these sources (e.g. Bian & Fan 2020; Meštrić et al. 2020) and the high opacity of the IGM during the EoR. Based on known samples of Lyman break galaxies (LBGs; Steidel et al. 2018) and Lyman α emitters (LAEs; Fletcher et al. 2019), Bassett et al. (2021) predict that Ly C emission from the bulk of star-forming galaxies at $z \geq 3.0$ should be fainter than 28 mag AB. The low flux of ionizing photons reaching the Earth is predominantly the result of absorption by hydrogen both within the host galaxy's interstellar medium (ISM), the circumgalactic medium (CGM), and the intervening IGM. The ISM/CGM absorption is directly related to the escape fraction of Ly C photons $f_{\rm esc}$, the measurement of which is the primary goal of a number of observational programs (e.g. Marchi et al. 2017; Wang et al. 2021). Variations in $f_{\rm esc}$ with other galaxy properties such as mass (e.g. Naidu et al. 2020), size and morphology (e.g. Kim et al. 2021), or time-varying star formation rate (Smith et al. 2019) can have significant implications regarding how the reionization process proceeds.

In order to measure such dependence on $f_{\rm esc}$ and galaxy properties, we must first be able to accurately estimate $f_{\rm esc}$ from observations.

★ E-mail: rbassett@swin.edu.au (RB); eryanweber@swin.edu.au (EVR-W)
† Canada Research Chair.

The largest difficulty in achieving this goal is the highly stochastic transmission of the IGM to ionizing photons (e.g. Inoue & Iwata 2008; Steidel et al. 2018; Bassett et al. 2021) as this quantity is degenerate with the value of f_{esc} inferred from observations. One strategy is to assume the average IGM transmission across a large ensemble of simulated transmission curves (e.g. Inoue et al. 2014), although this technique is likely to be appropriate only for statistically significant samples of Ly C detections, which are currently lacking. One can also apply each IGM transmission curve from an ensemble individually and provide a histogram of the resulting f_{esc} values (e.g. Shapley et al. 2016; Vanzella et al. 2016), though this alone provides poor constraint on f_{esc} and produces a large number of sightlines with $f_{esc} > 1$ (i.e. more Ly C photons escape the galaxy than are expected to be intrinsically produced). Future telescopes and instruments (e.g. the Keck Wide-Field Imager; Gillingham et al. 2020) are expected to push Ly C observations to greater depths, thus we may be on the cusp of the era of large Ly C samples. In light of this, it is important to reassess the methodology of estimating f_{esc} from observed galaxies.

In this paper, we aim to provide a statistical framework for determining the posterior probability distribution function (PDF) for f_{esc} from individual Ly C detected galaxies. This method applies an ensemble of 10 000 IGM transmission curves and tests 10 000 f_{esc} values for each of these possible sightlines, measuring the resulting Ly C flux for an ensemble of spectral energy distributions (SEDs) fit using a large grid of BPASSv2.1 (Eldridge et al. 2017) models. The modelled fluxes are considered in a probabilistic manner combining both the observed Ly C flux and uncertainty as well as the goodness of fit of each BPASS model to 20 photometric bands at $\lambda_{rest} > 1216$ Å (thus avoiding light attenuated by the IGM) producing a single f_{esc} PDF. The paper is organized as follows: in Section 2, we outline the sample selection and observations; in Section 3, we discuss the methodology including redshift measurement, providing a discussion of systematic overestimates of photometric redshifts (likely resulting from our selection criteria) then focus f_{esc} estimates for a single galaxy at $z > 3.4$; in Section 4, we present the results of our analysis for this galaxy, and in Section 5 we summarize our findings.

2 SAMPLE SELECTION AND OBSERVATIONS

All but one of the Ly C emitting candidate galaxies in our preliminary sample were selected from the ZFOURGE survey (PI Labbe; Straatman et al. 2016) for spectroscopic observations with the Multi-Object Spectrometer For Infra-Red Exploration (MOSFIRE; McLean et al. 2012). The ZFOURGE survey provides robust photometric redshifts by utilizing 30+ photometric bands from u^* band to far-infrared. The ZFOURGE team has estimated an average photometric redshift accuracy of ±2 per cent based on subsamples of galaxies with spectroscopic follow-up observations. It is relevant to point out that the photometric redshift accuracy quoted by ZFOURGE is primarily based on galaxies at $z < 3$ where the split *J*- and *H*-band filters probe the Balmer break directly. At higher redshifts, the Balmer break moves into the *K* band, thus the photometric redshifts are likely to become less reliable (see also Appendix A). The final galaxy in our sample is selected from the VIMOS Ultra Deep Survey (VUDS; Le Fèvre et al. 2015, ID 511227001), and already has a secure spectroscopic redshift measurement of $z = 3.64$. We carried out spectroscopic observations using MOSFIRE to confirm ZFOURGE photometric redshifts for the remaining targets (see Section 3.1).

Accurate redshifts are critical as our key selection criteria for Ly C emitting candidates is clean *u*-band detection (see e.g. Bassett et al. 2019), probing Ly C flux above $z \sim 3$ (exclusively so above $z = 3.4$). As in previous works (e.g. Bassett et al. 2019; Meštrić et al. 2020) *u*-band data come from the CFHT Large Area U-band Deep Survey (CLAUDS; Sawicki et al. 2019), which reaches a maximum depth of ∼27.2–27.3 mag in the *u* band. We note that the *u* band used here for Ly C detections is distinct from the u^* band of the ZFOURGE survey. In particular, the *u* band for the CLAUDS survey exhibits a sharp cutoff in transmission on the red end and does not suffer from red leak, a major drawback of the u^* band for Ly C studies.

All targets have available, multiband *Hubble Space Telescope* (*HST*) photometric data and for each we have performed visual comparison between *HST F*814*W* and the CLAUDS *u*-band imaging to exclude targets with a likely companion in the space-based imaging not apparent from the ground. The criteria for excluding galaxies based on this visual inspection are the presence of either multiple *HST* detections associated with a single *u*-band detection or an offset between the *u*-band centroid and the *F*814*W* centroid larger than the *HST* PSF. From our experience performing *u*-band selections in the COSMOS field, we find roughly one-third of galaxies exhibit close pairs in higher resolution imaging (see Meštrić et al. 2020). Comparison between *u* band and *F*814*W* imaging is shown in Fig. 1 with contours in the upper panel illustrating the smoothed *HST* photometry. The field of view for each target is 5 × 5 square arcsec. This step provides more confidence that many of our Ly C emitting candidate galaxies do not have their *u*-band flux contaminated by lower redshift interlopers (e.g. Vanzella et al. 2010). However, some targets with multiple *HST* peaks have been included due to the limited field of view observable in a single MOSFIRE mask. Thus, our sample represents a set aimed to optimize a single MOSFIRE mask in the ZFOURGE-COSMOS field. More details of our *u*-band selection can be found in Meštrić et al. (2020).

Ly C emitting galaxy candidates considered in this work have been observed using the MOSFIRE instrument at the Keck Observatory (proposal ID 2018B_W151 PI Bassett). MOSFIRE observations were performed in two half nights of 2018 December in the same manner as for galaxies described in Bassett et al. (2019). We observed in the *H* and *K* bands with *K*-band observations targeting [O III] (λ5007 and λ4959 Å) and H β, and *H*-band observations targeting [O II] (λλ3727 Å). In both cases, we employed a 1.″0 slit and a ABBA dither pattern with a 1.″25 nod. *K*-band observations were performed on December 17th with 60 × 180 s exposures, a total of 3 h on source. The seeing for our *K*-band observations varied from ∼0.″5 to ∼0.″61. *H*-band data were collected on December 19th using 100 × 120 s exposures, a total of 3.3 h on source. Seeing conditions for our *H*-band observations were similar to those for *K* band. We reduced the data using a combination of the standard MOSFIRE PYTHON reduction package[1] as well as custom scripts for flux calibration. For more details on our data reduction process, see Bassett et al. (2019). Our final sample consist of seven ZFOURGE and one VUDS galaxy observed with MOSFIRE, as outlined in Table 1.

3 METHOD

3.1 MOSFIRE analysis

Our method for measuring emission-line fluxes is the same as decribed in section 4.1 of Bassett et al. (2019). We simultaneously fit all emission lines using Gaussian profiles where the σ of all profiles are assumed to be the same. In this way, we are able to fit for the galaxy redshift directly rather than fitting the Gaussian centroid of

[1] https://keck-datareductionpipelines.github.io/MosfireDRP/

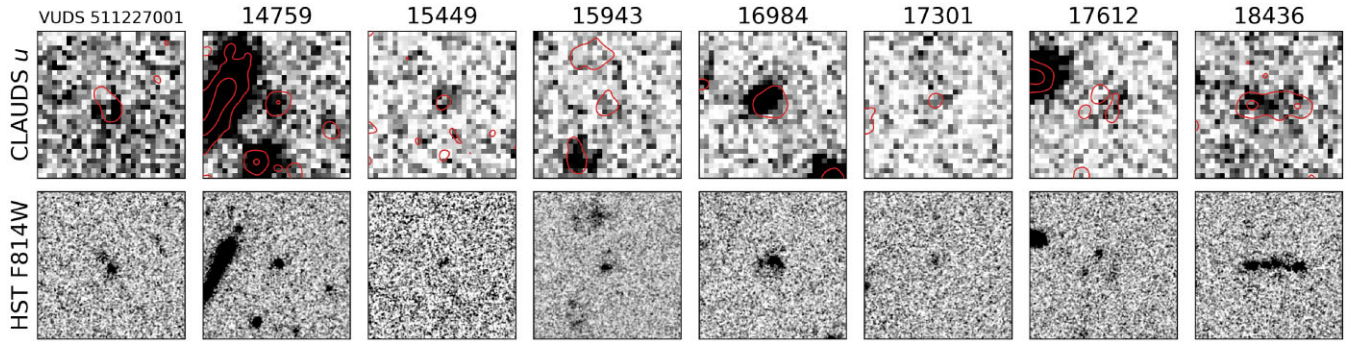

Figure 1. Imaging data used for sample selection with a field of view of 5 × 5 arcsec per cutout. *Top:* CLAUDS *u*-band imaging for our sample. Red contours are taken from the *HST F*814*W* imaging after smoothing with a Gaussian kernel with a width of 4 pixels. The purpose here is to illustrate the relative position of the source in each image. *Bottom: HST F*814*W* imaging of our sample with the same centring and field of view as for the top row.

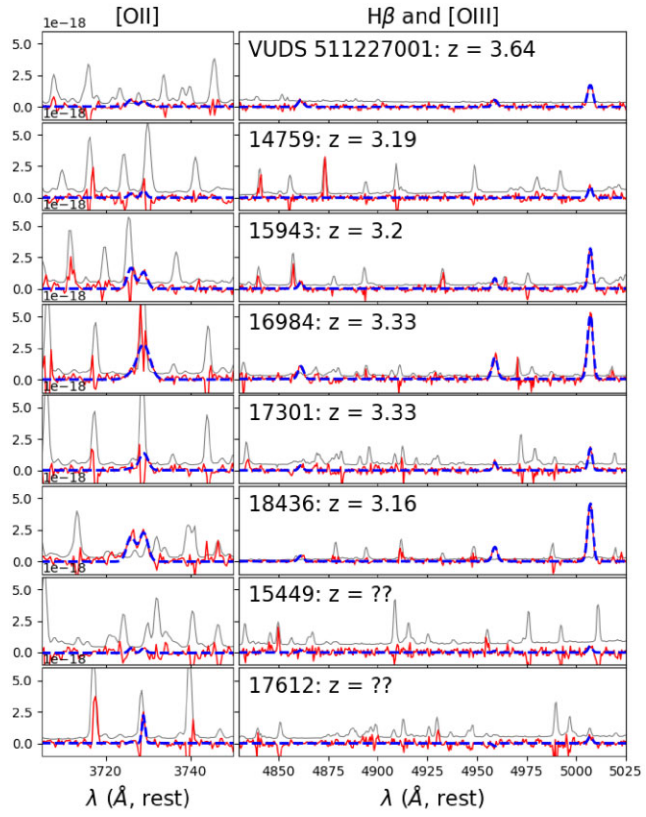

Figure 2. Fits to MOSFIRE observations of [O II] λλ3727, H β, [O III] λ4959, and [O III] λ5007 for our sample. The observed spectra and 1σ uncertainties are shown in red and grey, respectively, and our best-fitting model is shown in blue. The primary use of these data are to secure spectroscopic redshifts from for subsequent analysis of $f_{\rm esc}$. Galaxies 15449 and 17612 display marginal recovery of [O III] λ5007, thus we do not claim to have reliably secured spectroscopic redshifts for these targets. The remaining galaxies all display secure detections of [O III] λ5007, however.

each emission line separately. Thus, from our line-fitting procedure we extract the spectroscopic redshift, average σ for line-emitting gas, and the integrated line fluxes of the [O II] λλ3727 Å (MOSFIRE resolution provides only marginal separation of this doublet), H β, [O III] λ4959 Å, and [O III] λ5007 Å emission lines.

We show the emission-line fits for our sample in Fig. 2. For six out of eight targets, we detect [O III] λ4959 Å, [O III] λ5007 Å, and H β reliably enough to determine the spectroscopic redshift. Galaxies 15449 and 17612 provide unconvincing detections of [O III] λ5007, meaning we cannot obtain confident spectroscopic redshifts. These two targets are therefore omitted from further analysis. The recovery of other lines varies from target to target. In particular, the [O II] λλ3727 doublet often suffers from contamination from sky emission, which largely prohibits any meaningful line flux measurement. Regardless, the primary use of our MOSFIRE observations is to secure accurate redshifts and provide a basis for our *u*-band detections in the context of Ly C escape.

As stated in Section 2, our targets were specifically selected at $z > 3.4$ in order to ensure that the *u*-band detections probe Ly C photons exclusively. However, Fig. 2 shows that all of the targets selected from ZFOURGE based on photometric redshift estimates fall below this redshift cutoff. This means that our *u*-band detections contain contamination from Lyman α forest light. In general, our SED models contain significantly larger flux at $\lambda > 911.8$ Å when compared to Ly C wavelengths. Combined with the fact that we expect no correlation between the IGM transmission shortward of the Lyman limit and the transmission in the Lyman forest (e.g. Shapley et al. 2006; Bassett et al. 2021), we are unable to reliably constrain $f_{\rm esc}$ for galaxies at $z < 3.4$. Thus, the remaining ZFOURGE galaxies are removed from the sample for further analysis and only VUDS 511227001 will be considered in the context of Ly C escape.

The Ly C emission for VUDS511227001 has already been explored by Marchi et al. (2017), using VIMOS spectroscopy (1.3σ), and Meštrić et al. (2020). The latter study makes use of the same CLAUDS *u*-band observations used here in which VUDS 511227001 is detected at 27.82 mag (3.05σ). Although the *u* band probes bluer wavelengths than those probed by Marchi et al. (2017), where Ly C emission is expected to be weaker due to increased IGM attenuation, the increased depth of CLAUDS when compared to VIMOS mean these two observations are consistent. We estimate a limiting magnitude from the non-detection of Marchi et al. (2017; based on the conversion of the 1σ error of flux density) to be ∼26.6 mag, significantly brighter than the photometric detection presented here and in Meštrić et al. (2020), suggesting that the true brightness of VUDS511227001 was beyond the limit of VUDS.

3.2 SED models and dust attenuation

The remainder of this section is focused on estimating $f_{\rm esc}$ for the single target at $z > 3.4$, VUDS 511227001. The first step in this process is the selection of a model SED to which the observed *HST* and *u*-band photometry will be compared. Ultimately, the key property of any SED model in this context is the ratio of intrinsic

luminosity at 880–910 and 1450–1550 Å, $(L_{900}/L_{1500})_{\rm int}$. This is because the non-ionizing UV photometry provides the scaling for our SED model and $(L_{900}/L_{1500})_{\rm int}$ subsequently defines the intrinsic level of Ly C flux. The difference between this intrinsic flux and the observed u-band photometry will then define $f_{\rm esc}$. Given there is a high level of uncertainty regarding the specific star formation histories of high-redshift galaxies, here we employ a non-parametric SED fit using linear regression and BPASSv2.1 SED models (Eldridge et al. 2017) rather than constraining our models by assuming a fixed star formation history.

For VUDS511227001, we first extract the 31 photometric observations for from the COSMOS catalogues covering a rest wavelength range of ∼900–9600 Å. We also compile the filter transmission curves for all included filters. All photometric fluxes and associated errors are then converted to μJy and stored in an input table along with the MOSFIRE spectroscopic redshift. In our SED fitting, we exclude fluxes of any band with a rest wavelength shorter than 1216 Å as this probes the Ly C/Ly α forest portion of the specturm, thus the observed fluxes will also depend on $f_{\rm esc}$ and/or $T_{\rm IGM}$. This leaves 20 photometric fluxes for our SED fitting procedure. The SED fitting described here is primarily performed to constrain the intrinsic Ly C flux and $E(B-V)$, which are then used to independently estimate $f_{\rm esc}$ as described in Section 3.4.

Next, we prepare model photometric observations of BPASSv2.1 models, which will be used to assess the goodness of fit of each template. This is done by first converting the raw BPASS spectral models from their provided units (erg s^{-1} Å^{-1} 10^{-6} L$_\odot$) to μJy M$_\odot^{-1}$ at a given redshift. We then measure the weighted average flux per M$_\odot$ for each model in each photometric band from the COSMOS field where the weighting is given by the transmission curve of a given filter. 10 sets of BPASSv2.1 spectra are provided at metallicities between $z = 10^{-5}$ and $z = 0.014$ with each set containing 51 single stellar population (SSP) models in the age range $\log_{10}$(age) = 6–11 yr in bins of 0.1 dex. All metallicities are considered simultaneously while only the youngest 33 SSP ages are considered, as older SEDs would be older than the age of the Universe at the redshift of VUDS511227001. Thus, at each metallicity we produce a grid of 20 × 33 photometric fluxes with each row giving the photometric fluxes at a single age. Each individual grid is then stacked to produce a final grid of 200 × 33 photometric fluxes with each row representing an SED at a single age and metallicity. In all cases, we employ BPASSv2.1 models including binary stellar evolution, a power-law initial mass function (IMF), and an maximum stellar mass of 300 M$_\odot$ (see Eldridge et al. 2017, for more details), similar to other works considering Ly C emission at high redshift (e.g. Steidel et al. 2018).

We include dust attenuation in our SED fitting employing a Reddy et al. (2016) attenuation curve with $R_V = 2.74$. Generally, known Ly C emitting galaxies exhibit little or no dust attenuation (Vanzella et al. 2010, 2018; Shapley et al. 2016; Bian et al. 2017; Steidel et al. 2018), thus we test models with $E(B-V)$ values in the range 0.0–0.2 with $\Delta E(B-V) = 0.001$.

With our photometric grid and dust curves in place, our SED fitting procedure is performed. At each $E(B-V)$ value, we scale the photometric fluxes of the dust free grid to match the expected fluxes for our attenuation curve. We then use linear regression to determine the best-fitting linear combination of dust attenuated SSP templates. Our linear regression is achieved by minimizing the cost function $J(\Theta, X, Y, \sigma_Y)$ taken as the reduced χ^2 value:

$$J(\Theta, X, Y, \sigma_Y) = \frac{1}{2m}\sum_{i=1}^{m}\frac{(h(\Theta, X) - Y)^2}{\sigma_Y^2}, \quad (1)$$

where m is the number of photometric bands considered (20), X is the grid of model photometric fluxes, Y is the observed fluxes for a given object, and σ_Y is the associated measurement errors on the observed fluxes. Here, the function $h(\Theta, X)$ describes a 1D vector that represents the output SED where

$$h(\Theta, X)_i = \sum_{j=1}^{n}\Theta_j \times X_{j,i}, \quad (2)$$

where $n = 200$ is the number of different age/metallicity BPASSv2.1 SSP models considered. In this framework, and given our fluxes are in μJy per M$_\odot$, Θ can be seen as a vector describing the amount of stellar mass attributed to each SSP model of a given age with a length equal to the number of different aged models being considered at a given redshift. As an example, assume $i = 0$ corresponds to the B-band flux, thus $h(\Theta, X)_0$ represents the linear combination of B-band fluxes across all SSP ages with weighting given by the vector Θ.

The resulting best-fitting SED for a single realization of our fitting procedure will also depend on the initial conditions due to the nature of the optimization algorithm. We thus perform the fitting 250 times using a randomly initialized guess where the mass associated with each row is selected from a normal distribution with both μ and σ equal to 10^5 M$_\odot$. After initialization, any negative value is set to zero. Furthermore, the final values are constrained between 0 and 10^{10} M$_\odot$. We show the average output SED, which includes dust attenuation, in the top panel of Fig. 3 with the shaded area showing the 99th percentile range among all 250 fits. The average mass for each of the 330 single age stellar populations is shown in the bottom left of Fig. 3, which is representative of a typical fit result. As shown in Fig. 4, the resulting stellar mass falls in the range 4×10^{10} to 4.8×10^{10} M$_\odot$. We show the average star formation history in the bottom right panel of Fig. 3, which is found to by quite dynamic. Typical SED fits exhibit a strong burst roughly $10^{6.5}$ yr ago peaking above 200 M$_\odot$ yr^{-1}, and it is likely that this stellar population is the source of a majority of the Ly C emission originating in this galaxy. We also note that, although dust attenuation is typically relatively low as can be seen in Fig. 4, the intrinsic Ly C emission from SED fits with higher $E(B-V)$ is necessarily larger, which will be reflected in the estimated $f_{\rm esc}$ for such models.

It should be noted that the picture of star formation histories for massive galaxies at high redshift is highly uncertain. Although not presented here, we have also performed SED fits using exponentially declining and constant star formation histories, which result in a similar spectral shape. Thus, although the physical parameters such as M$_\odot$ and metallicity may vary depending on the details of star formation history, the intrinsic Ly C to UV flux, $(L_{900}/L_{1500})_{\rm int}$, is fairly consistent across all models. This value is one of the key drivers of the resulting estimate of $f_{\rm esc}$, meaning our results are not strongly dependent on our choice of star formation history.

3.3 IGM transmission

In order to produce PDFs of $f_{\rm esc}$ for VUDS 511227001 for each of the SED models described in Section 3.2, we need to also sample the PDF of the IGM transmission, $T_{\rm IGM}$, for the u band at that galaxy's redshift. Here, we produce 10 000 IGM transmission curves using the TAOIST-MC code,[2] based on the methods described in Inoue et al. (2014) and Steidel et al. (2018).

A full description of the methodology for producing IGM transmission curves can be found in Bassett et al. (2021), however,

[2]Available at https://github.com/robbassett/TAOIST_MC.

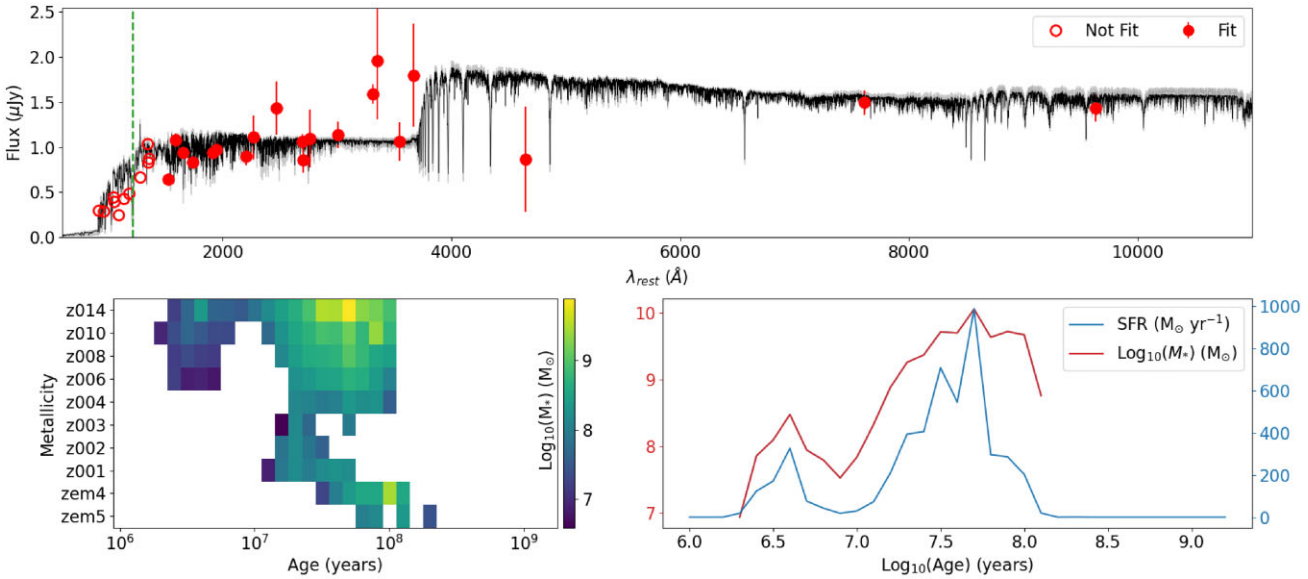

Figure 3. *Top:* SED fitting results for VUDS511227001. The average SED across our 250 fits is shown in black with the 99th percentile range shown as a shaded region. Solid red points show photometry included in the fitting procedure while open points show those that have been left out. These latter photometric observations are from filters that partially or entirely probe wavelength below Ly α (dashed vertical line) that are affected by IGM attenuation. *Bottom left:* The average stellar mass of each of our 330 single age, single metallicity BPASSv2.1 models across our 250 fits. The mass distribution represented here is typical of the majority of our fits. *Bottom right:* The average age versus stellar mass and star formation history of our SED fits. Typical star formation histories are dynamic and often characterized by a significant burst around $10^{6.5}$ yr ago peaking above 200 $M_\odot$ yr^{-1}. This recent burst is likely the primary contributor of Ly C photons to the galaxy's SED.

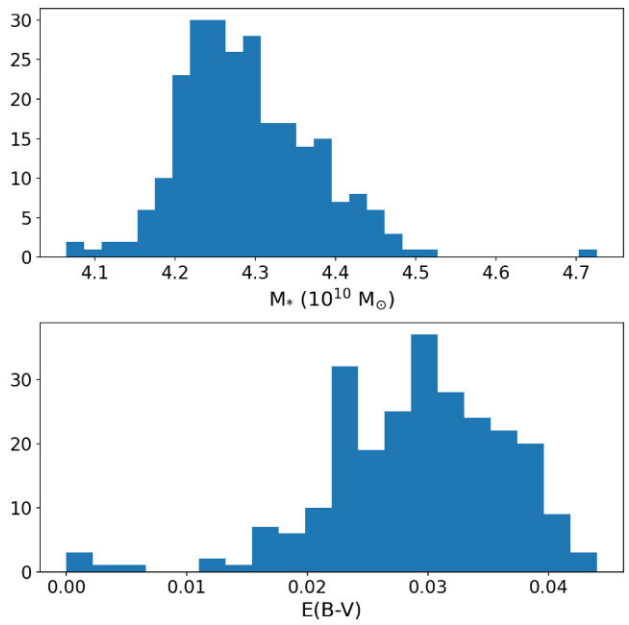

Figure 4. The distributions of stellar mass, top, and $E(B-V)$, bottom, for the 250 SED models produced in our fitting procedure. Both stellar mass and $E(B-V)$ are relatively consistent across the ensemble of models with the former found to be around $10 \times 10^{4.3}$ and the latter peaking around 0.03.

we briefly describe the major details here. For each stochastically produced IGM transmission curve, we first generate a single realization of possible intervening H I absorption systems in redshift bins of $\Delta z = 5 \times 10^{-5}$ from $z = 0$ to the redshift of VUDS 511227001, $z = 3.64$. Here, absorption systems are sampled from the 'IGM + CGM' column density distribution function presented in appendix B of Steidel et al. (2018). Next, for each absorption system, the transmission to ionizing radiation as a function of wavelength is determined at the particular redshift of that system. Finally, the cumulative IGM transmission function is computed as the combined transmission of all absorption systems from $z = 0$ to 3.64. This process is repeated 10 000 times to produce our ensemble of IGM transmission curves.

3.4 f_{esc} estimates

3.4.1 f_{esc} *from statistical analysis*

Having produced a series of SED models with similar goodness of fit and produced an ensemble of IGM transmission curves for VUDS 511227001, we now describe our method for determining the posterior PDF of f_{esc} for each model. The goal here is to determine the probability that the observed u-band flux and associated error is consistent with a given value of f_{esc} considering the ensembles of input SED models and IGM transmission curves described above.

For each of our 250 SED fits, we test all 10 000 IGM transmission curves, as well as 10 000 f_{esc} values between 0 and 1. We first multiply the intrinsic model spectrum (i.e. in the absence of dust attenuation) with a given IGM transmission curve, producing the SED + IGM model consistent with $f_{esc} = 1.0$. We then apply f_{esc} values between 0 and 1 with $\Delta f_{esc} = 1 \times 10^{-3}$. Here, we simply assume a flat transmission value for Ly C photons such that all photons with $\lambda_{rest} < 911.8$ Å are attenuated by the same value, namely the current f_{esc}. Next we measure the u-band flux of the SED + IGM + f_{esc} model by taking its weighted average with weighting given by the CLAUDS u-band transmission curve, which includes the combined effects of optics, CCD quantum efficiency, and the average atmospheric transmission at Mauna Kea. This value is taken as a single mock observation. We then determine the probability, P_{obs}, that a given

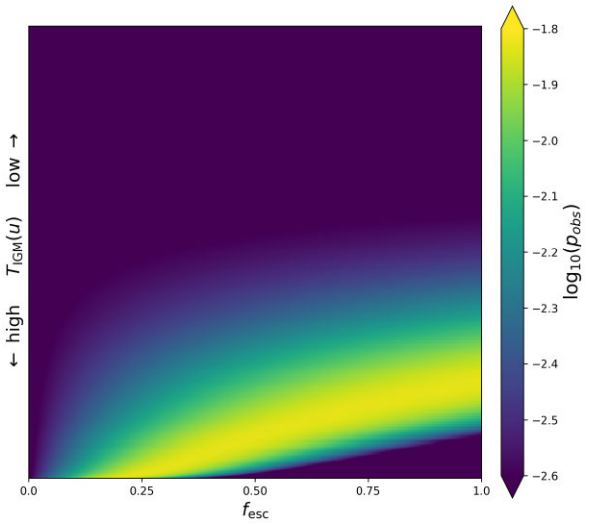

Figure 5. A 2D representation of the PDF of f_{esc} for 10 000 individual IGM sightlines for a single SED. Each row in this figure represents a single realization of the IGM transmission curve where we have ordered the rows in decreasing u-band transmission, $T_{IGM}(u)$, from bottom to top. As one might expect, the most probable value of f_{esc} for individual sightlines increases with decreasing IGM transmission. It can also be seen that for the majority of sightlines with relatively low transmission, the PDF is roughly flat with a value consistent with the probabilty for a u-band flux of 0. When computing the final f_{esc} PDF for each individual metallicity and age, we determine the probability of a single f_{esc} value by taking the median of this figure along the y-axis.

mock observation is consistent with the observation as the value of a Gaussian function with $F(u_0)$ and $\sigma(u)$ taken from the observed flux and error, respectively, evaluated at the position of the mock observation's $F(u)$.

This process is visualized for a single SED in Fig. 5 where each row represents a single IGM sightline and sightlines have been ordered by decreasing u-band IGM transmission from bottom to top. For each sightline, the colourbar shows the correspondence between a given f_{esc} value and P_{obs} where the highest value in a given row gives the f_{esc} value most consistent with the observed photometry. We note that for nearly half of our sightlines, the IGM transmission is so low that the resulting u-band flux is $\sim$0 for all f_{esc} meaning the value of P_{obs} is the same at all f_{esc}. In contrast, for the highest transmission sightlines at high f_{esc} the resulting u flux is more than twice the observed value meaning the combination of high transmission and high f_{esc} is less consistent with the observations than a u flux of 0 (see Section 4 for further discussion).

After applying all 10^8 combinations of T_{IGM} and f_{esc}, the probability of any individual value of f_{esc} is taken as the median across all 10 000 sightlines. This is equivalent to taking a one-dimensional median of Fig. 5 along the y-axis. In this way, we construct the PDF of f_{esc} for an individual combination of SED age, $E(B-V)$, and metallicity.

This process is repeated across the entire ensemble of SED models produced in Section 3.2, producing a broad ensemble of f_{esc} PDFs. We show all 250 f_{esc} PDFs in the top panel of Fig. 6 with the colour indicating the $E(B-V)$ value for a given model. We see the peak location of the PDF increases with decreasing $E(B-V)$. This relationship is shown in the bottom panel of Fig. 6 that shows a strong decrease from $f_{esc} = 1.0$ for models with $E(B-V) < 0.02$ down to $f_{esc} \simeq 0.3$ for our most attenuated model. This reflects the fact that the attenuated model is fit to the observed photometry while

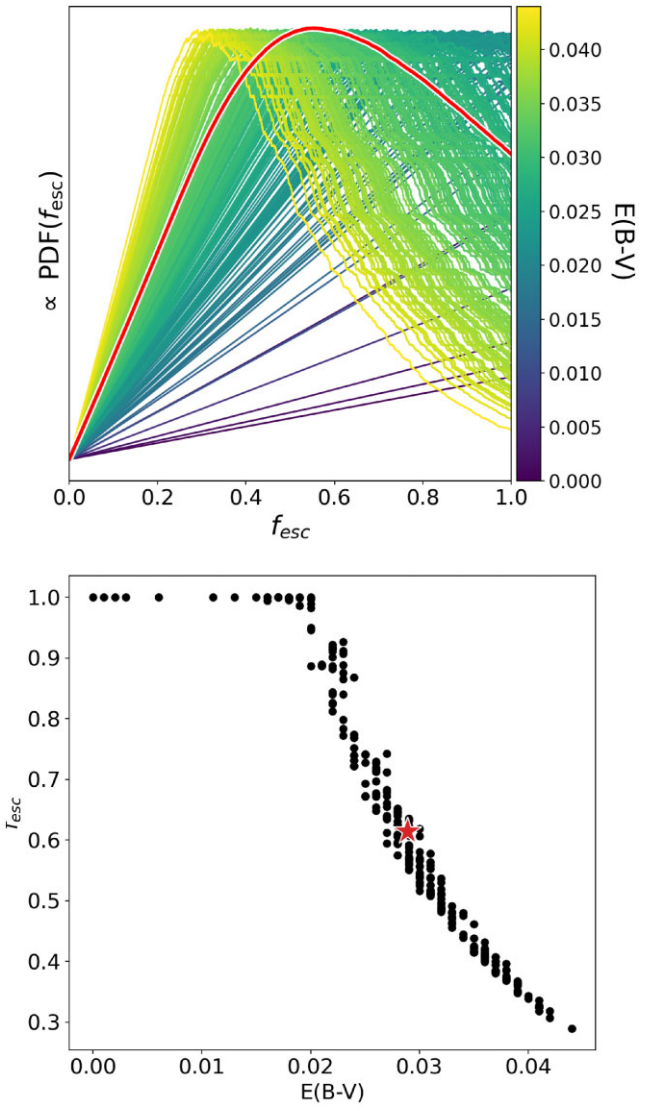

Figure 6. *Top:* Individual f_{esc} PDFs produced as described in Section 3.4 with colour indicating the $E(B-V)$ of a particular model. The average PDF across all 250 models is shown in red, and it is from this average PDF that we compute the median value and uncertainty of f_{esc} for VUDS511227001. *Bottom:* The relationship between the peak f_{esc} and $E(B-V)$ for each of our models. As can be inferred from the top panel, we find a decrease in f_{esc} with increasing $E(B-V)$. This is due to the fact that the intrinsic SED of a dust free model closely matches the observed photometry meaning a smaller difference between the intrinsic and observed LyC flux.

the intrinsic model has a higher flux with the difference increasing with $E(B-V)$.

We also produce a single f_{esc} PDF to consider the *entire* ensemble of models. This is achieved by taking the weighted average of all 250 PDFs with the weight given by the peak sum of a given PDF. This weighting scheme gives a lower weight to SEDs with low $E(B-V)$ as the peak, found at $f_{esc} = 1.0$; significantly below the peak value for models with maximums below $f_{esc} = 1.0$. We show the resulting average PDF in red in the top panel of Fig. 6.

It is from the weighted average f_{esc} PDF that we estimate the most probably value of f_{esc} for VUDS511227001. We also provide assymetric errors with the error on each side given by the difference between the most probable f_{esc} and the 15.9th and 84.1th percentiles,

roughly equivalent to the 1σ spread in the case of a Gaussian distribution. We also compare the value of $f_{\rm esc}$ computed using the method described here with $f_{\rm esc}$ computed for the same target using alternative methods (see below), thus for the remainder of this work this value of $f_{\rm esc}$ will be presented as $f_{\rm esc}^{\rm PDF}$. The resulting value of $f_{\rm esc}^{\rm PDF}$ from this process for VUDS 511227001 is $0.51^{+0.33}_{-0.34}$.

3.4.2 f_{esc} from average IGM transmission

A common method of estimating $f_{\rm esc}$ for Ly C detected galaxies is to assume $T_{\rm IGM}$ equal to the average value at a given redshift (Bian et al. 2017; Naidu et al. 2018; Fletcher et al. 2019). This method is more appropriately applied to large samples of Ly C detections as in this case differences in IGM sightline from galaxy to galaxy average out and an average value of $f_{\rm esc}$ can be estimated. To use the average IGM transmission in this way, however, requires large samples of Ly C detections at roughly fixed redshift. As such samples are not existent currently, the average transmission method has been applied to single galaxies in some previous works. While we do not advocate such an application, we calculate $f_{\rm esc}$ in this way for VUDS 511227001 for illustrative purposes. We note that, because we assume a CGM contribution to the attenuation of Ly C photons (following Steidel et al. 2018) the $f_{\rm esc}$ values estimated in this manner will be higher than if we had omitted this contribution (e.g. Inoue & Iwata 2008; Inoue et al. 2014).

Following a number of previous works (e.g. Steidel, Pettini & Adelberger 2001; Bassett et al. 2019; Meštrić et al. 2020), we calculate $f_{\rm esc}$ from the average IGM transmission in the following manner. We first calculate the so-called relative $f_{\rm esc}$, $f_{\rm esc}^{\rm rel}$ as

$$f_{\rm esc}^{\rm rel} = \frac{(F_{\rm LyC}/F_{1500})_{\rm obs}}{(L_{\rm LyC}/L_{1500})_{\rm int}} \times \frac{1}{\langle T_{\rm IGM}\rangle}, \quad (3)$$

where $(F_{\rm Ly\,C}/F_{1500})_{\rm obs}$ is the observed Ly C to 1500 Å flux ratio, $(L_{\rm Ly\,C}/L_{1500})_{\rm int}$ is the SED dependent, intrinsic Ly C to 1500 Å luminosity ratio, and $\langle T_{\rm IGM}\rangle$ is the transmission of the IGM to Ly C radiation measured here for the CLAUDS u band at the redshift of VUDS 511227001 of $z = 3.64$. We then convert $f_{\rm esc}^{\rm rel}$ to the absolute $f_{\rm esc}$, $f_{\rm esc}^{\rm abs}$, as

$$f_{\rm esc}^{\rm abs} = f_{\rm esc}^{\rm rel} \times 10^{-0.4(k_{1500}E(B-V))}, \quad (4)$$

where k_{1500} is the reddening at 1500 Å for our chosen Reddy et al. (2016) attenuation curve and $E(B-V)$ is the best-fitting value as calculated for each of our SED models in Section 3.2. For IGM transmission curves produced with TAOIST-IGM at $z = 3.641$, we find a value of $\langle T_{\rm IGM}\rangle$ for the u band of 0.04 ± 0.01.

Previous work has shown that for Ly C surveys, there is an expected bias such that the IGM transmission along sightlines towards Ly C detected galaxies is higher than the mean value (Rivera-Thorsen et al. 2019; Bassett et al. 2021). This bias, which we call $T_{\rm bias}$, is expected to vary depending on a variety of factors including observational depth, brightness of detected sources, and the intrinsic SED shape of observed sources (in particular the Ly C to 1500 Å flux ratio). While Bassett et al. (2021) primarily focused on quantifying $T_{\rm bias}$ for samples of Ly C detections, one can also compute the expected $T_{\rm bias}$ for individual detections. We note that, although IGM transmission is not an additive quantity, we prefer to define it as such for convenience. Thus, $T_{\rm bias}$ is defined as the difference between the average IGM transmission in sightlines in which a given galaxy is more likely to be observed and the average IGM transmission of all sightlines at a given redshift (see Bassett et al. 2021, for more details).

We demonstrate the bias in IGM transmission for VUDS 511227001 in Fig. 7. The black curve in each shows the unweighted mean transmission curve at $z = 3.64$ while coloured curves show the weighted average considering the observed photometry. Here, the weighting for each combination of SED and IGM transmission is determined by summing the resulting $f_{\rm esc}$ PDF for that combination (i.e. summing a single row in Fig. 5). The weighted average IGM transmission using this weigthing scheme is shown in Fig. 7 in cyan. To measure $T_{\rm bias}$, we take the weighted average of both curves in Fig. 7 with weights given by the CLAUDS u-band transmission curve and subtract the resulting value for the unweighted mean transmission from the biased mean transmission. $T_{\rm bias}$ for the CLAUDS u band for our 250 SED models is found to be 0.03 ± 0.01 giving $\langle T_{\rm IGM}\rangle + T_{\rm bias}$ 0.07 ± 0.02.

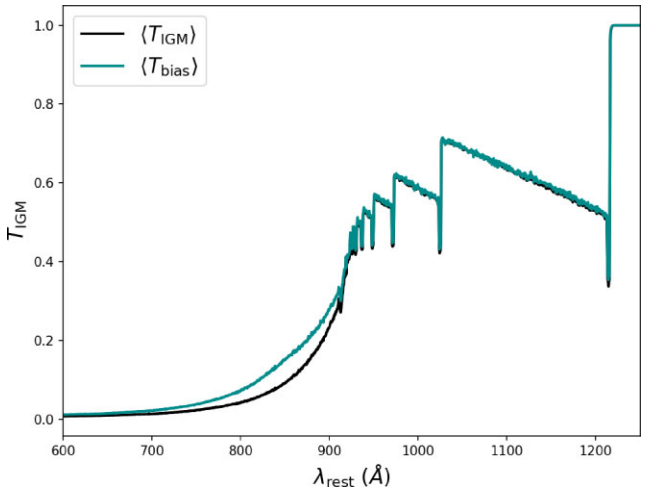

Figure 7. Shown in black is the average IGM transmission across all 10 000 simulated sightlines, while in cyan is shown the average biased transmission across all 250 SED models. For a single SED, the biased IGM transmission is calculated as the weighted average of all 10 000 sightlines with weight given by the sum of the $f_{\rm esc}$ PDF produced for each individual sightline (i.e. individual rows in Fig. 5). The average transmission in the u band for the biased transmission is 0.03 higher than the unweighted average transmission.

Having computed $T_{\rm bias}$ for each SED model, we can then compute a bias corrected value of $f_{\rm esc}$ as

$$f_{\rm esc}^{\rm bias} = \frac{(F_{\rm LyC}/F_{1500})_{\rm obs}}{(L_{\rm LyC}/L_{1500})_{\rm int}} \times \frac{1}{\langle T_{\rm IGM}\rangle + T_{\rm bias}}. \quad (5)$$

Although the level of $T_{\rm bias}$ expected for VUDS 511227001 appears negligible at ~0.03, estimating $f_{\rm esc}$ using equation (5) results in an appreciable difference when compared to equation (3).

For both $f_{\rm esc}^{\langle T\rangle}$ and $f_{\rm esc}^{\rm bias}$, the report values in Section 4 are taken as the mean across our 250 SED models. We also provide an assymetric error as the 15.9th and 84.1$^{\rm th}$ percentiles of the same 250 values. Given we are providing three different methods of calculating $f_{\rm esc}$, we distinguish these as $f_{\rm esc}^{\rm PDF}$ for the probability based method from Section 3.4.1, $f_{\rm esc}^{\langle T\rangle}$ for values calculated with equation (3), and $f_{\rm esc}^{\rm bias}$ for values calculated with equation (5), as demonstrated in Fig. 8. We reiterate that we consider $f_{\rm esc}^{\rm PDF}$ to be the most rigorous as it considers the sightline-to-sightline variation in $T_{\rm IGM}$, which typically has a more complex wavelength dependence than smooth curves produced by averaging over ensembles of sightlines. Our results suggest that these complex variations between individual sightlines can result in significant differences in calculated $f_{\rm esc}$ values and should be taken into account when interpreting detections of Ly C radiation from individual galaxies.

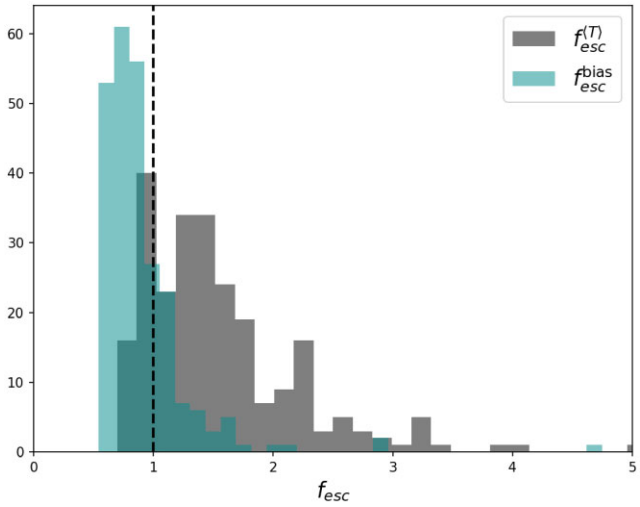

Figure 8. Histograms of $f_{\rm esc}^{\langle T\rangle}$ and $f_{\rm esc}^{\rm bias}$, the $f_{\rm esc}$ values estimated by assuming the average and the biased IGM transmission at the redshift of VUDS511227001. In the case of $f_{\rm esc}^{\langle T\rangle}$, the vast majority of $f_{\rm esc}$ values have unphysical values larger than 1. For $f_{\rm esc}^{\rm bias}$, the majority of values, as well as the average value, fall just below $f_{\rm esc} = 1$. Regardless, $f_{\rm esc}^{\rm bias}$ is significantly larger than $f_{\rm esc}^{\rm PDF}$ considering the modest average $T_{\rm bias}$ of 0.03.

4 RESULTS

In this section, we have a closer look at the PDFs of $f_{\rm esc}$ produced in Section 3.4 for VUDS 511227001. We begin by comparing the composite $f_{\rm esc}$ PDFs shown in Fig. 6, which take into consideration all 10 000 IGM sightlines, with $f_{\rm esc}$ PDFs produced for individual sightlines at a range of $T_{\rm IGM}$. Next, we will compare the final $f_{\rm esc}^{\rm PDF}$ values with the two more traditional $f_{\rm esc}$ estimates, $f_{\rm esc}^{\langle T\rangle}$ and $f_{\rm esc}^{\rm bias}$, produced from averaged IGM transmission curves. For clarity we state simply here that the resulting $f_{\rm esc}$ values of our three methods calculated for VUDS 511227001 are $f_{\rm esc}^{\rm PDF} = 0.51^{+0.33}_{-0.34}$, $f_{\rm esc}^{\langle T\rangle} = 1.40^{+0.80}_{-0.42}$, and $f_{\rm esc}^{\rm bias} = 0.82^{+0.33}_{-0.16}$. These values consider all 250 SED models produced in our analysis in a probabilistic manner (as described above).

In Fig. 9, we show $f_{\rm esc}$ PDFs of individual IGM for a single SED model. Shown are the 0th, 20th, 40th, 60th, 80th, and 100th percentiles in IGM transmission for the CLAUDS u band. We can see for sightlines with high IGM transmission the PDF is roughly Gaussian with the peak indicating the particular $f_{\rm esc}$ value exactly matching the observed u-band flux for a given sightline. Additionally, we see that the probability that 0 flux is consistent with the observed flux is ∼0.002, thus all sightlines overlap here for $f_{\rm esc}^{\rm PDF} = 0$. We also note that, as can be seen in Fig. 5, the majority of sightlines have a roughly flat PDF as the Ly C flux is ∼0, thus having a probability of ∼0.002, regardless of $f_{\rm esc}^{\rm PDF}$. In contrast, for sightlines with high IGM transmission, when $f_{\rm esc}^{\rm PDF}$ is large the resulting u-band flux is more than twice the observed value. This results in a $P_{\rm obs}$ value for such sightlines significantly lower than 0.002 (the value for $F(u) = 0$) meaning that the combination of high IGM transmission and high $f_{\rm esc}$ is less consistent with the observed value than a u flux of 0. This is precisely the reason that the median $P_{\rm obs}$ at high $f_{\rm esc}$ is lower than for intermediate values, resulting in a PDF that peaks below 1.

We also wish to point out that the final PDFs for $f_{\rm esc}^{\rm PDF}$ can vary significantly from the PDFs for any individual sightlines. The most transparent sightline, for instance, is roughly Gaussian and narrowly peaked with the most probable $f_{\rm esc}$ value at ∼0.19, significantly lower than the most probable value considering the full ensemble of IGM sightlines. Given any single galaxy exists along a single IGM sightline, were it possible to know the true transmission towards which VUDS 511227001 is observed the PDF would likely collapse to a more well-defined value. Further, if this sightline were of particularly high transmission, the most probable value would exist at a relatively low probability considering the ensemble PDFs shown

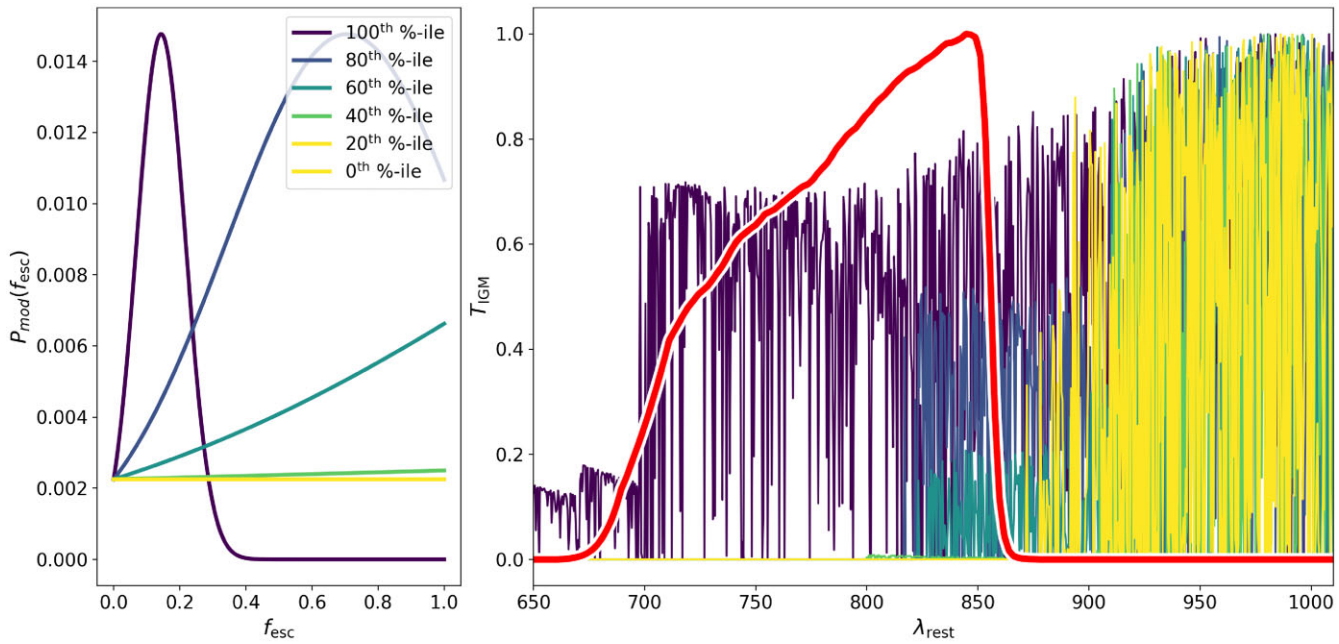

Figure 9. *Left:* The output probability distributions of $f_{\rm esc}$ for individual IGM sightlines covering a range in $\langle T_{\rm IGM}\rangle(u)$. Here, we have ordered all 10 000 sightlines by $\langle T_{\rm IGM}\rangle(u)$ and display the output PDF for percentiles between 0 and 100. Here, the 100th percentile represents the most transparent sightline in our analysis. *Right:* For reference the IGM transmission functions for each of the PDFs shown in the left-hand panel are displayed. We also show the trasmission of the u band, scaled to have a peak value of 1, in red.

Table 1. Results of our MOSFIRE analysis, all line fluxes in units of 1×10^{-18} erg s^{-1} cm^{-2}.

ID	RA	Dec.	z	f([O II] $\lambda\lambda$3727)	f(H β)	f([O III] λ4959)	f([O III] λ5007)
VUDS511227001	150.062182	2.423024	3.641	9.2 ± 5.5	8.7 ± 13.1	8.8 ± 8.4	28.1 ± 10.4
14759	150.0642853	2.3365283	3.189	<6.6	<4.2	<5.4	8.9 ± 8.1
15449	150.0592499	2.3442955	–	<7.5	<7.7	<8.2	<9.3
15943	150.0710449	2.3490129	3.202	<12.7	5.6 ± 13.6	9.1 ± 14.1	36.0 ± 13.5
16984	150.0836487	2.3587866	3.327	<14.8	15.3 ± 26.4	25.9 ± 28.7	75.6 ± 26.7
17301	150.0789032	2.3626015	3.325	<17.6	<8.7	<6.3	19.9 ± 8.4
17612	150.0817566	2.3652375	–	<4.5	<5.4	<7.8	<9.4
18436	150.0518951	2.3979318	3.156	44.1 ± 11.6	5.8 ± 25.4	15.1 ± 24.9	61.6 ± 23.6

Table 2. Median $f_{\rm esc}$ values for each of our different estimators. Assymetric represents the 15.9th and 84.1th percentile range, equivalent to 1σ for a Gaussian distribution.

$f_{\rm esc}^{\rm PDF}$	$f_{\rm esc}^{\langle T\rangle}$	$T_{\rm bias}$	$f_{\rm esc}^{\rm bias}$
$0.51^{+0.33}_{-0.34}$	$1.40^{+0.80}_{-0.42}$	$0.032^{+0.009}_{-0.010}$	$0.82^{+0.33}_{-0.16}$

in Fig. 6. This point must be kept in mind when consdering $f_{\rm esc}$ values for individual galaxies as it is likely that larger samples of Ly C detected galaxies are required to fully understand the role of star-forming galaxies in driving reionization.

We next compare $f_{\rm esc}^{\rm PDF}$ with the more traditional value of $f_{\rm esc}^{\langle T\rangle}$ and the value $f_{\rm esc}^{\rm bias}$, which takes into account the bias towards detecting galaxies from sightlines with non-zero IGM transmission. We can see in both cases that these two values result in significantly higher $f_{\rm esc}$ estimates when compared to $f_{\rm esc}^{\rm PDF}$, although $f_{\rm esc}^{\rm bias}$ is within the upper bounds of the 1σ spread in $f_{\rm esc}^{\rm PDF}$. Considering the final value that takes into account all metallicities and ages, bottom row of Table 2 (noting again this is most closely associated with our $Z_* = 0.14$ model), we find $f_{\rm esc}^{\rm PDF} = 0.51^{+0.34}_{-0.33}$, $f_{\rm esc}^{\langle T\rangle} = 1.40^{+0.80}_{-0.42}$, and $f_{\rm esc}^{\rm bias} = 0.82^{+0.33}_{-0.16}$. We note that estimates of $f_{\rm esc}$ for VUDS 511227001 have been performed previously by Meštrić et al. (2020, their galaxy ID 368) who provide a range of values for different $(L_{900}/L_{1500})_{\rm int}$. Our value of $1.40^{+0.80}_{-0.42}$ is consistent with the values presented in Meštrić et al. (2020) of $f_{\rm esc} \gtrsim 0.3$–0.93.

Considering the three calculations of $f_{\rm esc}$ presented here, we find that the values of $f_{\rm esc}^{\langle T\rangle}$ and $f_{\rm esc}^{\rm bias}$ here are larger than $f_{\rm esc}^{\rm PDF}$ by 0.88 and 0.30, respectively. It is also worth noting that $f_{\rm esc}^{\rm bias}$ is lower than $f_{\rm esc}^{\langle T\rangle}$ by 0.58, a significant decrease even though the average level of $T_{\rm bias}$ we calculated is small at $\sim$0.03. This further highlights the importance of carefully considering the fact that Ly C detections, by definition, are incompatible with IGM sightlines with very low or 0 transmission, which are often included in the calculation of $\langle T_{\rm IGM}\rangle$.

What then is the driver of the significant difference between $f_{\rm esc}^{\rm PDF}$ and both $f_{\rm esc}^{\langle T\rangle}$ and $f_{\rm esc}^{\rm bias}$? Ultimately, the determination of the probability of a given value of $f_{\rm esc}$ for an individual combination of IGM sightline and intrinsic SED shape is defined by the resulting u-band flux. Given that we use the same ensembles SED models for all $f_{\rm esc}$ determinations, we are left with the differing treatment of the IGM transmission. Clear differences can be seen by comparing average IGM transmission curves in Fig. 7 with individual curves from Fig. 9 with the former characterized by a smooth transition from high to low $T_{\rm IGM}$ with decreasing wavelength and the latter by sharp, stochastic drops in $T_{\rm IGM}$. Put another way, the smooth, average transmission curves commonly seen in the literature (e.g. Inoue et al. 2014; Steidel et al. 2018; Bassett et al. 2021) are not representative of individual sightlines and the stochastic nature of such individual transmission curves results in a posterior distribution of u-band fluxes that is not well captured assuming $\langle T_{\rm IGM}\rangle$ even when correcting for $T_{\rm bias}$. Some previous works (e.g. Shapley et al. 2016; Vanzella et al. 2016) have used ensembles of IGM transmission curves in their estimates of $f_{\rm esc}$ resulting in similar distributions of $\langle T_{\rm IGM}\rangle$ as seen here. Thus, the small novelty introduced in this work is the consideration of the observed flux and uncertainty to apply observational probabilities to individual sightlines resulting in a posterior $f_{\rm esc}$ distribution peaking below $f_{\rm esc} = 1.0$.

We end this section by reiterating that we consider this rigorous method of determining $f_{\rm esc}^{\rm PDF}$ to be most appropriate for determining $f_{\rm esc}$ for individual galaxies. This method takes into account the current best understanding of the probability of Ly C photons (at wavelengths where the u band is sensitive in the observed frame) encountering high column density neutral hydrogen along any individual line of sight. We repeat that the ensemble PDF produced this way may not be representative of the true PDF given any single galaxy has only one IGM transmission curve. What we have shown, however, is that methods considering only the mean IGM transmission, or even the biased average transmission (Bassett et al. 2021), are likely not providing reasonable estimates of individual $f_{\rm esc}$ values. Given the large uncertainties for individual estimates, however, it is most likely that statistically significant samples of Ly C detections will be required to truly understand the role of star-forming galaxies in reioinzation. Furthermore, it is also possible that the smooth, average transmission curves used to calculate $f_{\rm esc}^{\langle T\rangle}$ and $f_{\rm esc}^{\rm bias}$ are indeed appropriate when applied to larger samples of galaxies at roughly fixed redshift.

5 SUMMARY AND CONCLUSIONS

In this paper, we begin with a sample of eight galaxies selected as Ly C emitting candidates based on CLAUDS u-band detection. All of our targets were selected with prior redshift estimates at $z > 3.4$ such that the detected u-band flux can be attributed only to Ly C photons with $\lambda_{\rm rest} < 911.8$ Å. Previous redshift estimates for 7/8 of our sample come from ZFOURGE photometric analysis with the remaining galaxy selected from VUDS, which provides a secure spectroscopic redshift. Thus, we begin our analysis by measuring the spectroscopic redshifts of our ZFOURGE selected targets from [O III] λ5007 Å (along with [O III] λ4959 Å and H β, where detected) emission lines in Keck MOSFIRE spectroscopy.

Our first result is that all seven galaxies selected from ZFOURGE found to have overestimated photometric redshifts. In all cases, MOSFIRE spectroscopic redshifts are found at $z < 3.4$. This means that the u-band detections are contaminated by Lyman α forest photons, preventing us from providing meaningful constraints on the Ly C escape fraction $f_{\rm esc}$. Our systematic selection of galaxies

with overestimated photometric redshifts may suggest that our requirement of a *u*-band detection has resulted in a bias such that we preferentially select galaxies with overestimated photometric redshifts rather than clean detections of Ly C emission (see Appendix A). This result provides a useful warning to other projects searching for Ly C detections based only on photometric estimates of galaxy redshifts. Whether or not this is a general problem or related to the particular photometric bands and methods of the ZFOURGE survey or to any associated selection biases, however, is yet to be seen.

The final galaxy in our sample, VUDS 511227001 had a spectroscopic redshift estimate prior to our MOSFIRE observations. Our detections of [O III] λ5007 Å confirm the redshift of this target to be $z = 3.64$, thus its *u*-band detection results purely from Ly C photons. We reiterate that this galaxy has been analysed in the context of Ly C escape previously by Marchi et al. (2017, VIMOS spectroscopy) and Meštrić et al. (2020, also CLAUDS *u* band). For this target we have performed a rigorous statistical analysis to determine the PDF of $f_{\rm esc}$. In our analysis, we have produced 10 000 IGM transmission functions to $z = 3.64$ and employed an ensemble of 250 SED models constructed from BPASSv2.1 templates (see Section 3.2). Our SED models are non-parametric but have a characteristic mass of 4.25×10^{10} $M_{\odot}$ and exhibit bursty star formation histories. Critically, for determination of Ly C escape, these models cover a range of $(L_{900}/L_{1500})_{\rm int}$ between 0.02 and 0.15. We then produce PDFs of $f_{\rm esc}$ for each SED in a probablistic manner by applying all 10 000 IGM transmission functions across values of $f_{\rm esc}$ between 0 and 1 then taking into consideration the observed *u*-band flux and error of VUDS 5112270001 (for more details see Section 3.4.2). Finally, we determine a final PDF of $f_{\rm esc}$ across all 250 models as the weighted average of each individual PDF with weights given by the probability that a given SED matches the observed ZFOURGE photometry.

The final PDF of $f_{\rm esc}$ for VUDS 511227001 is shown in Fig. 6 in red, and we refer to the most probable value as $f_{\rm esc}^{\rm PDF}$. The resulting value for this target is $0.51^{+0.33}_{-0.34}$ where the asymmetric errors represent the 1σ range of our PDF. We also calculate two alternative values of $f_{\rm esc}$ using the mean IGM transmission, $\langle T_{\rm IGM}\rangle$, and mean transmission included the expected observational bias $\langle T_{\rm IGM}\rangle + T_{\rm bias}$ (see Bassett et al. 2021). These values, which we refer to as $f_{\rm esc}^{\langle T\rangle}$ and $f_{\rm esc}^{\rm bias}$ are found to be $1.40^{+0.80}_{-0.42}$ and $0.82^{+0.33}_{-0.16}$, respectively, noting that the expected level of bias in $\langle T_{\rm IGM}\rangle$ for this target is ∼0.03. The value calculated for $f_{\rm esc}^{\langle T\rangle}$ is consistent within errors with the previous estimate of Meštrić et al. (2020) who use a similar method. We postulate that the large differences between these estimates of $f_{\rm esc}$ result from the fact that individual IGM transmission functions are characterized by sharp drops not well represented by the smoothly declining functions seen in averaged IGM transmission curves. The complex shape of individual sightlines convolved with the SED model shape and the transmission of the *u* band result in a distribution of model *u*-band fluxes not well represented by the simplified calculations of $f_{\rm esc}^{\langle T\rangle}$ and $f_{\rm esc}^{\rm bias}$.

Ultimately, we also question the value of individual measurements of $f_{\rm esc}$, even using a rigorous method such as the one presented here. Any observation of a galaxy represents a single IGM transmission, and we have shown that knowing the exact form of this transmission can result in a PDF not well represented by the PDF we produce by marginalizing over 10 000 such sightlines. Thus, it is likely that a real understanding of the role of star-forming galaxies in cosmic reionization will require much larger samples of Ly C detected galaxies, and in such cases average transmission curves become more appropriate.

ACKNOWLEDGEMENTS

This research was conducted by the Australian Research Council Centre of Excellence for All Sky Astrophysics in 3 Dimensions (ASTRO 3D), through project number CE170100013. Some of these data were obtained and processed as part of the CFHT Large Area U-band Deep Survey (CLAUDS), which is a collaboration between astronomers from Canada, France, and China described in Sawicki et al. (2019). CLAUDS is based on observations obtained with MegaPrime/ MegaCam, a joint project of CFHT and CEA/DAPNIA, at the CFHT which is operated by the National Research Council (NRC) of Canada, the Institut National des Science de l'Univers of the Centre National de la Recherche Scientifique (CNRS) of France, and the University of Hawaii. CLAUDS uses data obtained in part through the Telescope Access Program (TAP), which has been funded by the National Astronomical Observatories, Chinese Academy of Sciences, and the Special Fund for Astronomy from the Ministry of Finance of China. CLAUDS uses data products from TERAPIX and the Canadian Astronomy Data Centre (CADC) and was carried out using resources from Compute Canada and Canadian Advanced Network For Astrophysical Research (CANFAR). (Some of) The data presented herein were obtained at the W. M. Keck Observatory, which is operated as a scientific partnership among the California Institute of Technology, the University of California and the National Aeronautics and Space Administration. The Observatory was made possible by the generous financial support of the W. M. Keck Foundation. The authors wish to recognize and acknowledge the very significant cultural role and reverence that the summit of Maunakea has always had within the indigenous Hawaiian community. We are most fortunate to have the opportunity to conduct observations from this mountain. Results presented in this work have made extensive use of the PYTHON3 programming language (Van Rossum & Drake 2009) and, in particular, the authors wish to acknowledge the NUMPY (Oliphant 2006), MATPLOTLIB (Hunter 2007), and SCIPY (Virtanen et al. 2020) packages. MR and LP acknowledge support from *HST* programs 15100 and 15647. Support for Program numbers 15100 and 15647 were provided by NASA through a grant from the Space Telescope Science Institute, which is operated by the Association of Universities for Research in Astronomy, Incorporated, under NASA contract NAS5-26555. MS acknowledges support from the Natural Sciences and Engineering Research Council (NSERC) of Canada.

DATA AVAILABILITY

IGM transmission functions used in this work is produced primarily using publicly available codes found at https://github.com/robbassett as well as publicly available galaxy SED models from the BPASS collaboration (Eldridge et al. 2017). Observational data from Keck are available from the Keck science archive and CLAUDS data will be released publicly in the near future (likely late 2021).

REFERENCES

Bassett R. et al., 2019, MNRAS, 483, 5223
Bassett R., Ryan-Weber E. V., Cooke J., Meštrić U., Kakiichi K., Prichard L., Rafelski M., 2021, MNRAS, 502, 108
Bian F., Fan X., 2020, MNRAS, 493, L65
Bian F., Fan X., McGreer I., Cai Z., Jiang L., 2017, ApJ, 837, L12
Bolton J. S., Haehnelt M. G., 2007, MNRAS, 382, 325
Eldridge J. J., Stanway E. R., Xiao L., McClelland L. A. S., Taylor G., Ng M., Greis S. M. L., Bray J. C., 2017, Publ. Astron. Soc. Aust., 34, e058
Fletcher T. J., Tang M., Robertson B. E., Nakajima K., Ellis R. S., Stark D. P., Inoue A., 2019, ApJ, 878, 87

Ghara R., Giri S. K., Ciardi B., Mellema G., Zaroubi S., 2021, MNRAS, 503, 4551
Gillingham P., Cooke J., Glazebrook K., Mould J., Smith R., Steidel C., 2020, in Ellis S. C., d'Orgeville C., eds, Proc. SPIE Conf. Ser. Vol. 11203, Advances in Optical Astronomical Instrumentation 2019. SPIE, Bellingham, p. 112030F
Grazian A. et al., 2018, A&A, 613, A44
Hunter J. D., 2007, Comput. Sci. Eng., 9, 90
Hutter A., Dayal P., Yepes G., Gottlöber S., Legrand L., Ucci G., 2021, MNRAS, 503, 3698
Inoue A. K., Iwata I., 2008, MNRAS, 387, 1681
Inoue A. K., Shimizu I., Iwata I., Tanaka M., 2014, MNRAS, 442, 1805
Kakiichi K. et al., 2018, MNRAS, 479, 43
Kim K. J., Malhotra S., Rhoads J. E., Yang H., 2021, ApJ, 914, 2
Le Fèvre O. et al., 2015, A&A, 576, A79
McLean I. S. et al., 2012, in McLean I. S., Ramsay S. K., Takami H., eds, Proc. SPIE Conf. Ser. Vol. 8446, Ground-based and Airborne Instrumentation for Astronomy IV. SPIE, Bellingham, p. 84460J
Marchi F. et al., 2017, A&A, 601, A73
Meštrić U. et al., 2020, MNRAS, 494, 4986
Naidu R. P., Forrest B., Oesch P. A., Tran K.-V. H., Holden B. P., 2018, MNRAS, 478, 791
Naidu R. P., Tacchella S., Mason C. A., Bose S., Oesch P. A., Conroy C., 2020, ApJ, 892, 109
Oliphant T., 2006, NumPy: A guide to NumPy. Trelgol Publishing, USA
Pagano M., Fronenberg H., 2021, MNRAS, 505, 2195
Planck Collaboration XLVII, 2016, A&A, 596, A108
Reddy N. A., Steidel C. C., Pettini M., Bogosavljević M., Shapley A. E., 2016, ApJ, 828, 108
Rivera-Thorsen T. E. et al., 2019, Science, 366, 738
Robertson B. E., Ellis R. S., Furlanetto S. R., Dunlop J. S., 2015, ApJ, 802, L19
Sawicki M. et al., 2019, MNRAS, 489, 5202
Shapley A. E., Steidel C. C., Pettini M., Adelberger K. L., Erb D. K., 2006, ApJ, 651, 688
Shapley A. E., Steidel C. C., Strom A. L., Bogosavljević M., Reddy N. A., Siana B., Mostardi R. E., Rudie G. C., 2016, ApJ, 826, L24
Shivaei I. et al., 2018, ApJ, 855, 42
Smith A., Ma X., Bromm V., Finkelstein S. L., Hopkins P. F., Faucher-Giguère C.-A., Kereš D., 2019, MNRAS, 484, 39
Steidel C. C., Pettini M., Adelberger K. L., 2001, ApJ, 546, 665
Steidel C. C., Bogosavlevic M., Shapley A. E., Reddy N. A., Rudie G. C., Pettini M., Trainor R. F., Strom A. L., 2018, ApJ, 869, 123
Straatman C. M. S. et al., 2016, ApJ, 830, 51
Tran K.-V. H. et al., 2020, ApJ, 898, 45
Vanzella E., Siana B., Cristiani S., Nonino M., 2010, MNRAS, 404, 1672
Vanzella E. et al., 2016, ApJ, 825, 41
Vanzella E. et al., 2018, MNRAS, 476, L15
Van Rossum G., Drake F. L., 2009, Python 3 Reference Manual. CreateSpace, Scotts Valley, CA
Virtanen P. et al., 2020, Nat. Methods, 17, 261
Wang B. et al., 2021, ApJ, 916, 3

APPENDIX A: SYSTEMATICALLY OVERESTIMATED PHOTOMETRIC REDSHIFT FOR *u*-BAND SELECTED GALAXIES

Here, we take a closer look at the systematic overestimate of ZFOURGE photometric redshifts for all seven galaxies selected based on those redshifts. In all cases, this overestimate was large enough that the true redshift, based on [O III] 5007 Å detections, was found to be below $z \lesssim 3.4$, the redshift limit for CLAUDS-*u* to cleanly sample the Ly C emission. As we have stated, this finding ultimately means that estimates of f_{esc} from the *u*-band detections for these galaxies are almost entirely unconstrained.

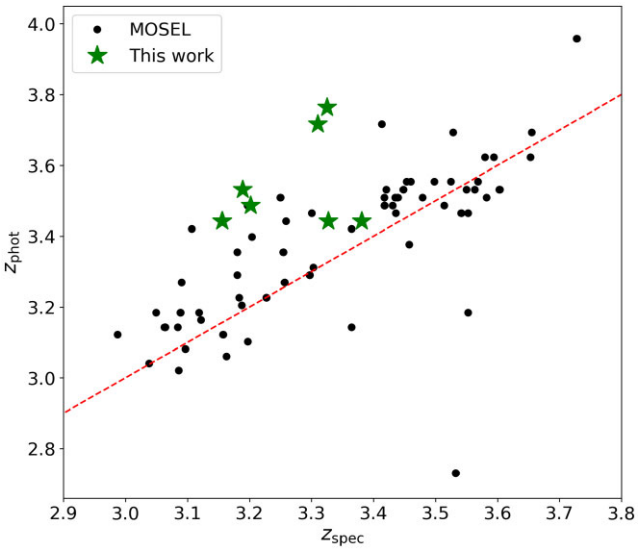

Figure A1. Photometric versus spectroscopic redshift measurements for our sample and a sample of MOSEL (Tran et al. 2020) galaxies at a similar redshift. Here, we show that 7/7 of our ZFOURGE targets are found to have overestimated photometric redshift estimates from the ZFOURGE catalog. In comparison, 47/70 of the MOSEL galaxies have similarly overestimated photometric redshifts. If we take MOSEL as a parent sample, we find a probability of 0.062 that we have selected seven galaxies with overestimated photometric redshifts by chance. We postulate instead that our selection criteria, in particular the requiredment of a detection in the CLAUDS *u* band, have resulted in a bias towards selecting galaxies with overestimated photometric redshifts.

These targets provide a useful cautionary result regarding Ly C candidate selection based on the combination of photometric redshift and expected Ly C detection. The question we pose here is: is it possible that our sample selection methodology has induced a bias such that we are more likely to select galaxies with overestimated photometric redshifts from the ZFOURGE survey? Indeed, the photometric redshift accuracy quoted by the ZFOURGE team based on spectroscopic follow up is $\lesssim$2 per cent with roughly equal mix of under and overestimated photometric redshift (e.g. Straatman et al. 2016). We reiterate that this statement is based primarily on lower redshift galaxies where the ZFOURGE medium band filters directly probe the Balmer break, which is not the case at the redshift of our sample. This would suggest that our selection of 7/7 galaxies with overestimated photometric redshifts is statistically unlikely from random selection alone.

To test for a statistical effect, we have obtained a sample of 70 ZFOURGE galaxies at $z > 3$ having spectroscopic follow-up observations taken from the Multi-Object Spectroscopic Emission Line survey (MOSEL; Tran et al. 2020). We show in Fig. A1 a comparison between photometric and spectroscopic redshifts for both MOSEL galaxies (black circles) and our sample (green stars). The sample of MOSEL galaxies shown here represents the largest sample of ZFOURGE galaxies at $z > 3$ with measured z_{spec} currently known, thus we will use this sample to determine the likelihood that spectroscopic redshift versus photometric redshift for our sample is consistent with a random selection from ZFOURGE.

From Fig. A1 it can be seen that, similar to our sample, there is a tendency for ZFOURGE photometric redshift to be slightly overestimated at $z > 3$. Indeed, 47/70 galaxies in the MOSEL sample have overestimated photometric redshift. To determine if our selection of 7/7 overestimated photometric redshift is consistent

with a random sampling of MOSEL galaxies we employ binomial statistics: either galaxies have underestimated photometric redshift or they do not. From this simple test, we can calculate the probability of selecting seven out of seven galaxies with overestimated photometric redshift among $z > 3$ galaxies in ZFOURGE as $P(k; n, p) = (47/70)^7$, giving 0.062. Furthermore, we note that the five out of seven of our ZFOURGE targets are found near the upper limit of $z_{\rm phot}$ - $z_{\rm spec}$ of the MOSEL sample meaning the true probability of selecting galaxies with such a large photometric redshift overestimate is even less likely than the simple binary statistics estimate presented here. Thus, we consider it improbable that we have selected seven galaxies with overestimated photometric redshift by chance.

An alternative explanation is a bias induced by our selection requirements: $z_{\rm phot} > 3.4$, lack of close companions in space-based imaging, and a clear detection in the CLAUDS *u* band. For a given galaxy to satisfy the final requirement of *u*-band detection, at least one of three things must be true. Either the galaxy truly is a high-redshift Ly C emitter, the detection is contaminated by a low-redshift interloper unresolved even in *HST* imaging, or the photometric redshift is overestimated and the *u*-band detection is contaminated by brighter Ly α forest emission. Given the high spatial resolution of *HST* imaging, the second possibility is unlikely. The liklihood of finding true Ly C emitters is still somewhat uncertain with detections rates in recent surveys in the 5–20 per cent rate (Steidel et al. 2018; Fletcher et al. 2019; Meštrić et al. 2020), with possible dependence on selection type (i.e. LBG versus LAE; e.g. Bassett et al. 2021). Based on the fact that >2/3 of MOSEL galaxies have overestimated photometric redshifts, the liklihood of a biased selection of galaxies with overestimated photometric redshifts is more likely than selection of true Ly C emitters with our ZFOURGE + CLAUDS selection. Thus, we conclude that our selection aimed at identifying Ly C emitters at $z > 3.4$ based solely on photometric redshifts has induced a selection bias that undermines our efforts at measuring $f_{\rm esc}$ at high-z.

This paper has been typeset from a TEX/LATEX file prepared by the author.